Crossover in the wetting behavior at surfactant-laden liquid-crystal–water interfaces: Experiment and theory

Erfan Kadivar,* Christian Bahr,† and Holger Stark‡

Max Planck Institute for Dynamics and Self-Organization, Bunsenstr. 10, D-37073 Göttingen, Germany

The behavior of a nematic liquid crystal at a surfactant-laden interface to an aqueous phase is studied under the condition of homeotropic anchoring. It is shown that with decreasing surfactant concentration the system shifts from surface-enhanced to surface-decreased order, i.e., the behavior changes from complete nematic wetting when the nematic–isotropic phase transition is approached from above to a different wetting behavior below the transition, characterized by a considerably decreased Maier-Saupe order parameter at the interface. The experimental behavior is analyzed within the framework of the Landau–de Gennes theory supplemented by a surface free energy, in which the wetting behavior is controlled by the magnitude of the anchoring strength and the preferred surface order parameter in comparison to the bulk order parameter. The theoretical modeling is able to account for all experimental observations.

PACS number(s): 61.30.Hn, 64.70.Md, 68.05.Cf

I. INTRODUCTION

Thermotropic liquid crystals exhibit a wealth of surface phenomena related to wetting and anchoring (for reviews, see [1,2]). Anchoring describes the orientation of the liquid crystal director $\mathbf{n}$ (the average direction of the long molecular axis of the rodlike molecules) at an interface. Common anchoring states observed in experimental systems are homeotropic anchoring ($\mathbf{n}$ being parallel to the interface normal $\mathbf{z}$), planar unidirectional anchoring ($\mathbf{n} \perp \mathbf{z}$ in connection with a preferred in-plane direction of $\mathbf{n}$), and planar degenerate anchoring ($\mathbf{n} \perp \mathbf{z}$ with all in-plane directions being equivalent).

Landau–de Gennes models [3–7] and microscopic theories [8–14] predict a large variety of pretransitional wetting behaviors depending on the different anchoring situations at an interface. They can be described by means of three cases [1], namely (I) strong or medium homeotropic anchoring, (II) strong or medium planar anchoring, and (III) weak anchoring with a possible anchoring transition between homeotropic and planar ordering.

For case I systems, the presence of a thin nematic- or smecticlike layer (with $\mathbf{n} \| \mathbf{z}$) is predicted in the temperature range well above the bulk liquid-crystal to isotropic phase transition temperature T_b. If the temperature is decreased towards T_b, the thickness of the ordered interface layer should diverge corresponding to complete wetting of the isotropic bulk phase by the liquid-crystal phase. For medium homeotropic anchoring strengths, partial wetting (i.e., the thickness of the wetting layer stays finite as T_b is approached) should occur. This behavior has been experimentally confirmed and was widely studied at plane interfaces to air [15–18] and

various substrates [19–28] as well as in cylindrical pores [2,29–31]. For isotropic–nematic transitions, both complete and partial wetting can be found; for isotropic–smectic transitions, mainly the partial wetting behavior is observed and the wetting layer increases by a finite number of layering steps.

For case II, a similar scenario of complete or partial liquid-crystal (with $\mathbf{n} \perp \mathbf{z}$) wetting above T_b is expected, which may be complicated by the possible occurrence of biaxial surface phases. However, corresponding experimental systems, showing, e.g., complete wetting of the isotropic phase by a planar nematic layer, have not been observed to date. Experimental systems with planar anchoring show above T_b either no pretransitonal wetting at all [25,26] or a thin layer with a negative nematic order parameter [2,32]. This behavior is expected for the planar side of case III. Both homeotropic and planar case III systems are also expected to show a less-ordered or isotropic wetting layer below T_b which should grow as T_b is approached from below. In other words, the anchoring situation should determine the wetting behavior: For strong or medium anchoring, the system should exhibit enhanced surface order and a more-ordered surface phase should wet the less-ordered bulk phase above T_b, whereas for weak anchoring (close to a planar–homeotropic anchoring transition), decreased surface order is expected and a less-ordered surface phase should wet a more-ordered bulk phase below T_b. Experimentally, wetting by a less-ordered layer has been observed only on the planar side of an anchoring transition [32]. We report here the first experimental example of a system with homeotropic anchoring, in which a less-ordered wetting layer appears which grows in thickness as T_b is approached from below.

Surfactants are a useful tool for experimental realizations of anchoring transitions at interfaces to solid substrates [26] as well as to aqueous phases: Whereas planar anchoring exists at interfaces to pure water, the presence of surfactants with the common polar head or nonpolar tail structure leads to homeotropic anchoring, if the surfactant concentration exceeds a certain value [33]. Thus, an anchoring transition from planar to homeotropic can be realized by increasing the

*Present address: University of Isfahan, Department of Physics, 81746 Isfahan, Iran.
†christian.bahr@ds.mpg.de
‡Present address: Technical University Berlin, Institute of Theoretical Physics, Hardenbergstr. 36, D-10623 Berlin, Germany; holger.stark@ds.mpg.de
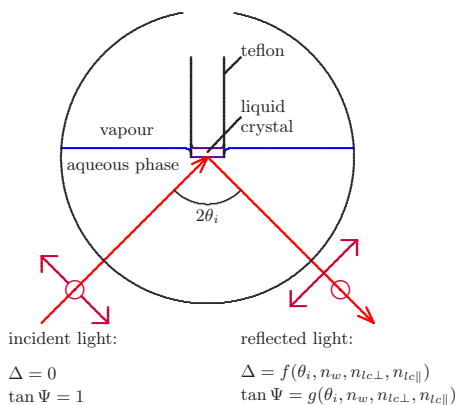
FIG. 1. (Color online) Schematic setup for ellipsometric measurements at the interface between thermotropic liquid crystals and aqueous phases. The ellipsometric parameters Δ and Ψ of the reflected light depend on the angle of incidence θ_i and the refractive index profile of the interface.

surfactant concentration at liquid crystal–water interfaces. We have recently demonstrated that at such interfaces a nematic wetting layer ($\boldsymbol{n} \| \boldsymbol{z}$) exists above T_b for sufficiently strong homeotropic anchoring and that the strength of the ordering surface field can be controlled by the variation of the surfactant concentration in the aqueous phase [34].

In the present study, we consider the behavior in this system at low surfactant concentrations where the anchoring is still homeotropic but close to the transition to planar anchoring. We show that with decreasing surfactant concentration the wetting behavior changes from nematic wetting above T_b to a different wetting phenomenon below T_b which is characterized by a considerably decreased nematic order parameter at the interface to the aqueous phase. The thickness of this decreased order parameter region increases as T_b is approached from below. We show that a theoretical model based on the Landau–de Gennes theory, in which the influence of the interface is described by two quantities, anchoring strength γ and preferred surface order parameter S_0, is able to describe the experimentally observed behaviors above and below T_b. Using one set of bulk parameters, we are able to fit all the experimental data. In addition, we determine the path in the γ, S_0 plane, on which the experimental system is moving as the surfactant concentration is decreased and also clarify at which surfactant concentration our system exhibits partial or complete wetting when the phase transition is approached. Thus, as we demonstrate now in detail, our combined experimental and theoretical investigation offers a clear picture of the wetting behavior at surfactant-laden liquid-crystal–water interfaces in the case of homeotropic anchoring.

II. EXPERIMENT

We study the liquid-crystal compound 8CB (4-octyl-4′-cyanobiphenyl); the material was bought from Synthon Chemicals, Germany, and used as received. The bulk nematic–isotropic transition temperature T_b of 8CB is at 41 °C. Figure 1 gives a schematic of our sample cell. The

liquid crystal is contained in a teflon tube (diameter 7 mm) which dips into a reservoir with an aqueous solution of the surfactant CTAB (hexadecyltrimethylammonium bromide; bought from Aldrich and used as received). The thickness of the liquid-crystal sample amounts to several mm, so that the liquid-crystal–air interface is well separated from liquid-crystal–water interface. Since the aqueous phase does not intrude between the organic liquid crystal and the teflon surface, it is possible to tune the curvature of the liquid-crystal–water interface by adjusting the immersion depth of the teflon tube and a plane interface, suitable for ellipsometric measurements, can be prepared. The interface is located in the center of a spherical glas container which is placed in a copper oven allowing for optical access of the incident and reflected laser beam of the ellipsometer.

The temperature of the sample is controlled with a resolution of ≈ 0.02 K. A phase-modulated ellipsometer is used to determine the magnitude $\tan \Psi$ and the argument Δ of the complex amplitude ratio $r_p/r_s = \tan \Psi \exp(i\Delta)$ of the p- and s-polarized components of the laser beam ($\lambda = 633$ nm) which is reflected from the liquid-crystal–water interface. Since the adsorption of the surfactant at the interface needs some time, the sample is allowed to equilibrate for a certain period before a measurement of the temperature dependence is started. This period ranges from several hours at larger CTAB concentrations to several days at very low CTAB concentrations; the equilibration is monitored by measuring the ellipsometric parameters at a fixed temperature just above the nematic–isotropic bulk transition until the values stay constant.

For the measurements of the temperature dependence, data are continuously collected while the temperature is changed at a slow constant rate (typically 0.02 K/min). The angle of incidence θ_i is permanently adjusted so that the value of Δ is between 85° and 95°. Under this condition, θ_i is a good approximation of the Brewster angle θ_B and the value of $\tan \Psi$, then designated as ellipticity coefficient $\bar{\rho}$, is most sensitive to the presence of an interface layer which differs in its optical properties from the two bulk media. The relative accuracy of our $\bar{\rho}$ and θ_B values is better than 1%, however, the absolute accuracy is of the order of 5% since errors or imperfections from several sources (calibration of the ellipsometer, alignment of the optical components, adjustment of the interface of the sample) add up.

Figure 2 shows examples of the experimentally determined temperature dependencies of $\bar{\rho}$ and θ_B for different CTAB concentrations c_a in the aqueous bulk phase. The behavior at concentrations $c_a \geq 0.8$ μM has already been analyzed in [34]; in this concentration range, corresponding to the type I case (strong or medium homeotropic anchoring), the interface is wetted above T_b by a nematic film which shows a pronounced, divergent growth in thickness as $T \rightarrow T_b$ as theoretical modeling reveals. This behavior is illustrated by the pronounced growth of $\bar{\rho}$ in Fig. 2(a) which shows the data for $c_a = 0.8$ μM. Lowering the surfactant concentration results in marked changes of $\bar{\rho}(T)$. Figures 2(b)–2(d) show the experimental data for $c_a = 0.7$ μM, 0.6 μM, and 0.4 μM. It is obvious that the pretransitional increase of $\bar{\rho}$ above T_b becomes less pronounced and finally vanishes as c_a is decreased to 0.4 μM. On the other hand, for
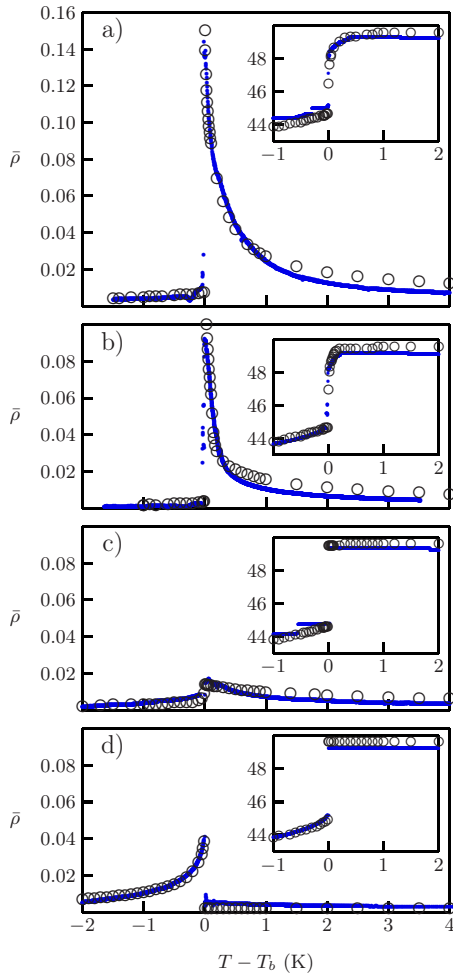
FIG. 2. (Color online) Temperature dependence of ellipticity coefficient $\bar{\rho}$ for different CTAB concentrations: (a) 0.8 μM, (b) 0.7 μM, (c) 0.6 μM, and (d) 0.4 μM. Solid lines or small dots are experimental data; open circles are calculated values resulting from the theoretical model described in Sec. III. The insets show the temperature dependence of the Brewster angle θ_B; y units: deg; x units: K.

this concentration a pretransitional increase of $\bar{\rho}$ is now observed as T_b is approached from *below*. For the sample, with $c_a = 0.6$ μM, a pronounced increase of $\bar{\rho}$ is observed on neither side of T_b.

The behavior of the Brewster angle θ_B is consistent to that of $\bar{\rho}$. Although θ_B is less sensitive to the presence of thin interface layers, it clearly exhibits pretransitional effects above T_b for the 0.8 μM and 0.7 μM samples. In the 0.6 μM and 0.4 μM samples, θ_B is constant above T_b (below T_b, the temperature dependence of the nematic bulk order parameter masks any pretransitional effects in θ_B). It is important to note that θ_B decreases for all samples by $\approx 4°$ at T_b, which unambiguously indicates a homeotropic anchoring of the nematic director for all samples (planar anchoring would result in an increase or, depending on the in-plane director orientation, in a constant behavior of θ_B). The homeotropic anchoring is also confirmed by the absence of any fluctuations in the measured $\bar{\rho}$ and θ_B values, which are to be expected if the director possesses a nonzero in-plane compo-

nent, and which are indeed observed when the aqueous phase consists of pure water [34].

From the data presented in Fig. 2 one can draw already some qualitative conclusions: The 8CB/CTAB/H_2O system shows above T_b complete wetting of the isotropic liquid-crystal–aqueous interface by a nematic layer for $c_a \geq 0.7$ μM [34]. If c_a is decreased to 0.4 μM, an indication of a pretransitional wetting above T_b is no longer observed, i.e., the complete wetting behavior has been replaced by a nonwetting situation. This happens without changing the kind of anchoring which is homeotropic for all CTAB concentrations down to 0.4 μM. The vanishing of the nematic wetting above T_b is accompanied by the appearance of a different pretransitional wetting phenomenon below T_b. The ellipsometric data of the wetting behavior below T_b can be qualitatively reproduced by a simple slab model, in which the interface between the aqueous phase and the nematic bulk phase is wetted by a nematic layer possessing an order parameter which is considerably smaller than that of the nematic bulk phase.

In the following section, we present a theoretical model based on the Landau–de Gennes theory which can reproduce the experimentally observed behavior above and below T_b for all CTAB concentrations. As a result, we are able to connect these concentrations to parameters of the theory, namely the surface anchoring strength γ and the preferred order parameter S_0 at the surface. In addition, the modeling will clarify where, in the experiment, complete or partial wetting occurs. It will also show that the nematic order parameter of the 0.4 μM sample [Fig. 2(d)] close to T_b is decreased at the interface by more than 70% compared to the bulk value and the thickness of the decreased order parameter region between the aqueous interface and the bulk nematic phase amounts to ≈ 30 nm. This means that we are close to the case what would be called a "disordering surface."

III. THEORY: WETTING OF A PLANAR INTERFACE

We summarize here the theory needed to study both wetting of an interface with nematic order when the nematic-isotropic phase transition is approached from above and suppression of nematic order or wetting of the interface with the isotropic phase when the phase transition is approached from below. In concrete, we investigate the orientational order of a nematic liquid crystal in a semi-infinite space ($z \geq 0$) induced by a bounding planar interface at $z = 0$.

In general, the surface-induced orientational order is quantified by a traceless and symmetric second-rank tensor $\boldsymbol{Q}$ [35–38], also called the alignment tensor [39]. Starting from a microscopic level, it is defined by $Q_{ij} = \langle \hat{\nu}_i \hat{\nu}_j - \frac{1}{3}\delta_{ij}\rangle$, where the unit vector $\hat{\nu}$ indicates the directions of single molecules and $\langle \cdots \rangle$ means average over all molecules in a sufficiently large volume. Our experiments show that the water–liquid-crystal interface with a sufficient amount of surfactant induces uniaxial ordering of the liquid-crystal molecules in the bulk with a uniform director field $\boldsymbol{n}(\boldsymbol{x}) = \boldsymbol{e}_z$ oriented along the surface normal commonly referred to as homeotropic anchoring of the molecules. So we can unambiguously choose an uniaxial order parameter $Q_{ij}(z)$

$= \widetilde{S}(e_{zi}e_{zj} - \frac{1}{3}\delta_{ij})$, where $\widetilde{S}(z)$ is the Maier-Saupe order parameter.

A. Free energy

Using this $Q_{ij}(z)$ in the Landau–Ginzburg–de Gennes free energy density [40,41], we arrive at the free energy per unit area in terms of the order parameter profile $\widetilde{S}(z)$:

$$\widetilde{F}_A[S(z)] = \int_0^\infty \left[\frac{1}{3}a_0(T - T^*)\widetilde{S}^2 - \frac{2}{27}b\widetilde{S}^3 + \frac{1}{9}c\widetilde{S}^4 \right.$$
$$\left. + \frac{1}{3}L_1\left(\frac{d\widetilde{S}}{dz}\right)^2 \right]dz + \frac{W}{3}[\widetilde{S}(0) - \widetilde{S}_0]^2, \quad (1)$$

where T is temperature and T^* denotes the supercooling temperature of the isotropic phase. In addition, we introduced a surface potential $\widetilde{F}_S = (W/3)[\widetilde{S}(0) - \widetilde{S}_0]^2$ with the preferred order parameter $\widetilde{S}_0$ at the surface and the surface-coupling strength $W > 0$ that penalizes any deviation of $\widetilde{S}(0)$ from $\widetilde{S}_0$. Note that the surface potential differs from the one used by Sheng in his seminal work on the boundary layer transition [3]. A wetting diagram for nematic wetting on the basis of $\widetilde{F}_S$ was published only recently [6]. Furthermore, $\widetilde{F}_S$ is crucial for being able to fit all of our experimental curves in Sec. II with one set of bulk parameters a_0, T^*, b, c, and L_1. We checked that this was not possible with the simpler surface potential used by Sheng.

The number of parameters in Eq. (1) is reduced considerably and thus theoretical analysis is simplified by using a rescaled order parameter $S = \widetilde{S}/r$ $[r = 2\sqrt{6}b/9c]$ and temperature $\tau = a_0(T - T^*)/cr^2$. Furthermore, all lengths and the free energy density are given, respectively, in units of $\xi = \sqrt{L_1/cr^2}$ and $\Delta f = cr^4/3$, where $2\sqrt{2}\xi$ denotes the nematic coherence length at the nematic-isotropic phase transition. Introducing also the dimensionless surface-coupling parameter $\gamma = W\xi/L_1$, which quantifies the competition between surface and elastic free energy, the reduced free energy per unit area reads

$$F_A[S(z)] = \int_0^\infty \left[f_b + \left(\frac{dS}{dz}\right)^2 \right]dz + \gamma[S(0) - S_0]^2 \quad (2)$$

with the bulk free energy density

$$f_b = \tau S^2 - \frac{1}{\sqrt{6}}S^3 + \frac{1}{3}S^4. \quad (3)$$

Note that by rescaling the free energy $\widetilde{F}_A$, we are left with only three essential parameters: Temperature τ, preferred order parameter S_0, and surface anchoring strength γ that completely determine the wetting behavior of the liquid crystal. Furthermore, according to the bulk free energy density f_b, the bulk nematic-isotropic phase transition from $S = 0$ to $S_b = \sqrt{6}/4 \approx 0.612$ occurs at $\tau_b = 1/8$, and $\tau^\dagger = 9/64$ is the superheating temperature of the nematic phase.

Based on free energy F_A, we will study wetting both for surface-induced prolate order ($S > 0$), where the liquid crystal molecules align preferentially along the surface normal, but also for oblate order ($S < 0$), where they want to be parallel to the interface. However, the second case has to be treated with caution since one expects biaxial orientational ordering as several theoretical studies for temperatures above τ_b have already shown [4,7,42–46].

B. General formalism

Variation of the free energy (2) in order to determine the order parameter profile $S(z)$ that minimizes F_A gives the Euler-Lagrange equation for the bulk,

$$\frac{d^2S}{dz^2} = \frac{1}{2}\frac{df_b}{dS}, \quad (4)$$

and the two boundary conditions at the interface,

$$\left.\frac{dS}{dz}\right|_{z=0} = \gamma[S(0) - S_0], \quad (5)$$

and far from it,

$$\left.\frac{dS}{dz}\right|_{z\to\infty} = 0 \quad \text{or} \quad \lim_{z\to\infty} S(z) = S_\infty. \quad (6)$$

For $z \to \infty$ the orientational order is uniform and the bulk value S_∞ is determined by minimizing the bulk free energy density f_b of Eq. (3). Integrating the Euler-Lagrange equation (4) once and determining the integration constant from boundary condition (6), gives

$$\left|\frac{dS}{dz}\right| = \sqrt{f_b(S) - f_b(S_\infty)}. \quad (7)$$

Finally, this formula together with boundary condition (5) at the interface, determines the order parameter $S(0)$ at the interface:

$$\gamma|S(0) - S_0| = \sqrt{f_b(S(0)) - f_b(S_\infty)}. \quad (8)$$

For $\tau \leq \tau_b$, Figures 3(a) and 3(b) illustrate graphical representations of Eq. (8) for $0 < S_0 < S_b$ and $S_0 < 0$, respectively. Note that in this case $f_b(S_\infty) \leq 0$. When multiple solutions for $S(0)$ occur, the absolute minimum of the free energy F_A has to be determined. Combining Eqs. (2) and (7) and using a transformation of the integration variable from z to S under the reasonable assumption that $S(z)$ is monotonic, one ultimately arrives at

$$F_A = K \pm 2\int_{S(0)}^{S_\infty} [\sqrt{f_b(S) - f_b(S_\infty)} \mp \gamma(S - S_0)]dS, \quad (9)$$

with the constant $K = f_b(S_\infty)d - \gamma(S_\infty - S_0)^2$, where d is the sample thickness in units of ξ and $f_b(S_\infty)d$ is the bulk free energy, when the whole sample would exhibit bulk order [3]. The upper and lower signs refer to $dS/dz \geq 0$ and $dS/dz \leq 0$, respectively. The first case occurs, e.g., for $\tau \leq \tau_b$ when $S(z)$ approaches S_∞ starting from $S(0) < S_\infty$ and the second case applies to $\tau \geq \tau_b$ when $S(z) > 0$ decays monotonically to $S_\infty = 0$. For the situation illustrated in Fig. 3(b), a graphical representation of F_A is possible: The free energies
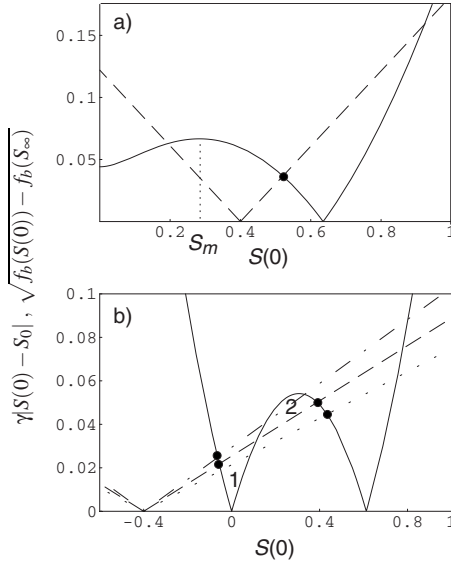
FIG. 3. Graphical solution of Eq. (8) for (a) $\tau < \tau_b$ and $0 < S_0 < S_b$ or (b) $\tau = \tau_b$ and $S_0 < 0$. The straight lines correspond to $\gamma|S(0) - S_0|$ and the curved to $\sqrt{f_b(S(0)) - f_b(S_\infty)}$. The dots indicate the absolute minimum of the free energy F_A. In (b) the free energies of the first three solutions differ by the areas 1 and 2 enclosed by the curved and one of the straight lines. With increasing γ, a parameter value is passed where the areas 1 and 2 are equal (Maxwell construction) and where the absolute minimum $S(0)$ jumps from a positive to a negative value.

of the different solutions $S_i(0)$ differ by the areas 1 and 2 enclosed by the curved and one of the straight lines. The dots indicate the absolute minimum of the free energy F_A. So if the areas are equal (reminiscent to the Maxwell construction), a (pre)wetting transition between different wetting profiles occurs. In Fig. 3(a) such a graphical representation of F_A does not exist, but after a careful inspection one is able to show that solutions of the type marked by the dot always correspond to the absolute minimum.

Once $S(0)$ is known, the concrete profile $S(z)$ follows from the implicit equation
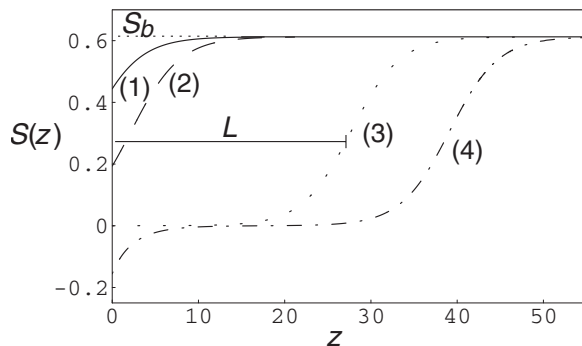
FIG. 4. Order parameter profiles $S(z)$ for isotropic wetting close to or at the bulk phase transition temperature τ_b for different surface parameters: (1) $S_0 = 0.3$, $\gamma = 0.3$, $\tau = \tau_b$; (2) $S_0 = 0.1$, $\gamma = 0.5$, $\tau = \tau_b$; (3) $S_0 = 10^{-5}$, $\gamma = 0.5$, $\tau = \tau_b$; (4) $S_0 = -0.5$, $\gamma = 0.2$, $\tau = 0.124\,999\,9$. The thickness L of the wetting layer is defined by the inflection point farthest away from the interface at $z = 0$. The coordinate z is given in units of ξ, which in our experiments is around 2.84 nm.
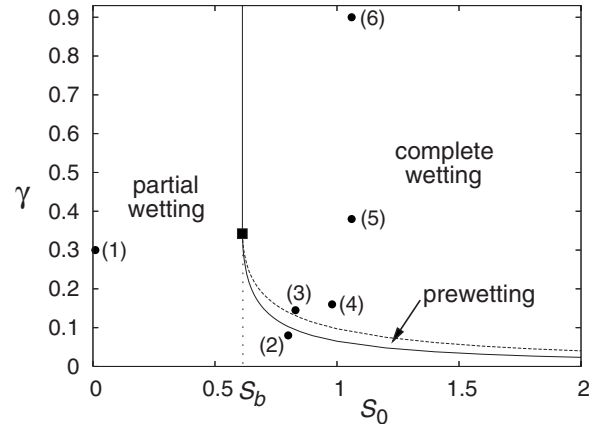
FIG. 5. Wetting phase diagram for nematic wetting when τ_b is approached from above. It is a projection of the full S_0, τ, γ wetting diagram onto the S_0, γ plane at τ_b. S_b is the bulk order parameter right at the phase transition. The filled square indicates a tricritical point for the wetting transitions at $(S_0 = S_b, \gamma = \sqrt{\tau_b} = 0.354)$. A detailed description is given in the main text. The dots correspond to parameter values obtained by fitting the experimental curves (cf. Fig. 2) for the temperature dependence of the ellipticity coefficient $\bar{\rho}$ and Brewster angle θ_B for different surfactant concentrations c_a: (1) 0.4 μM, (2) 0.6 μM, (3) 0.7 μM, (4) 0.8 μM, (5) 3 μM, and (6) 30 μM.

$$z = \pm \int_{S(0)}^{S(z)} \frac{dS}{\sqrt{f_b(S) - f_b(S_\infty)}}, \qquad (10)$$

where Eq. (7) was integrated from the interface to z. Different examples for such profiles are illustrated in Fig. 4 for $\tau \leq \tau_b$. Complete wetting of the interface with an isotropic phase can occur for $\tau \to \tau_b$ when $S(0) \leq 0$ [see curve (4) in Fig. 4] since at the phase transition $f_b(S=0) = f_b(S_\infty = S_b)$. So a macroscopically thick layer of isotropic liquid close to the interface is allowed for energetical reasons. To quantify the thickness of wetting layers, we note that every extremum S_m in the bulk free energy f_b gives rise to an inflection point in the profile $S(z)$ as stated by the the Euler-Lagrange equation (4). We define the thickness L of a wetting layer by the distance of the inflection point from the interface:

$$L = \pm \int_{S(0)}^{S_m} \frac{dS}{\sqrt{f_b(S) - f_b(S_\infty)}}. \qquad (11)$$

If two inflection points exist, the one with the largest distance is chosen. Whenever $f_b(S)$ approaches $f_b(S_\infty)$, a singularity occurs in the definition (11) and L diverges as we will demonstrate for $\tau \leq \tau_b$ in Sec. III D.

C. Nematic wetting on approaching the nematic-isotropic phase transition from above

Wetting of a planar interface with a uniaxial nematic order when the nematic-isotropic phase transition is approached from above is a well-studied problem since the first work by Sheng [3]. One of the authors has recently published a three-dimensional wetting phase diagram depending on temperature and the two parameters of the surface free energy in Eq.
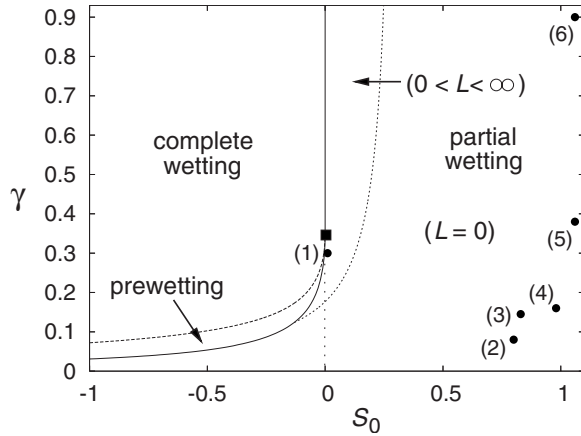
FIG. 6. Wetting diagram for isotropic wetting when τ_b is approached from below. It is a projection of the full S_0, τ, γ wetting diagram onto the S_0, γ plane at τ_b. The filled square indicates a tricritical point for the wetting transitions at $(S_0=0, \gamma=\sqrt{\tau_b} =0.354)$. A detailed description is given in the main text. The dots correspond to parameter values obtained by fitting the experimental curves (cf. Fig. 2) for the temperature dependence of the ellipticity coefficient $\bar{\rho}$ and Brewster angle θ_B for different surfactant concentrations c_a: (1) 0.4 μM, (2) 0.6 μM, (3) 0.7 μM, (4) 0.8 μM, (5) 3 μM, and (6) 30 μM.

(2) [6]. We shortly review it here in Fig. 5 as a projection along the temperature axis on the S_0, γ plane located at the phase transition temperature $\tau=\tau_b$. We especially want to demonstrate where the surfactant-laden water–liquid-crystal interfaces in our experiments are located in this diagram.

The full line in Fig. 5 separates the regions of complete and partial wetting. In the first case, a macroscopically thick nematic layer develops close to the interface when the bulk phase transition is approached with decreasing temperature, whereas in the second case the nematic film only has a microscopic thickness. The dashed line is the projection of a critical line on the S_0, γ plane at τ_b. It terminates a prewetting surface in the full S_0, τ, γ wetting diagram. When crossing this surface with decreasing temperature, the order parameter profile jumps from the thin to the thick-film solution before its thickness diverges at temperature τ_b. When crossing at τ_b the curved full line $(S_0 > S_b)$ in Fig. 5 from below, a first-order wetting transition occurs; whereas the transition is second order when the vertical full line at $S_0=S_b$ is traversed from the left, i.e., the thickness of the nematic film at $\tau=\tau_b$ diverges when the vertical line is approached from $S_0 < S_b$. So the filled square in Fig. 5 indicates a tricritical point. It is located at $(S_0=S_b, \gamma=\sqrt{\tau_b}=0.354)$.

D. Isotropic wetting on approaching the nematic-isotropic phase transition from below

Here we discuss the possibility that the isotropic phase can wet the interface when the nematic-isotropic phase transition is approached from below, i.e., when the bulk phase is in the nematic state. Figure 6 presents the relevant wetting phase diagram in the parameter space of the surface potential. Again, it is a projection of the full S_0, τ, γ wetting dia-

gram onto the S_0, γ plane at τ_b. It looks very similar to the diagram for nematic wetting illustrated in Fig. 5. Indeed the full line, indicating the wetting transitions, results from the analogous line in Fig. 5 when mirrored at $S_0=S_b/2$. It separates again a region of complete from a region of partial wetting. In the second case, the nematic order parameter close to the interface is reduced relative to the bulk value S_∞ (for $S_0 < S_\infty$) but never reaches 0 in order to be able to completely wet the interface with the isotropic phase. The dashed line in the partial-wetting regime divides a region where the wetting layer, following our definition (11), has zero thickness L from a region with $L \neq 0$. In the case of $L=0$, the maximum S_m in the free energy is smaller than $S(0)$ (see Fig. 3) so that the profile $S(z)$ does not have an inflection point; see curve (1) in Fig. 4 as an example. In Fig. 6 the separating line is given for $\tau=\tau_b$. For arbitrary temperatures $\tau < \tau_b$, it is determined by using $S(0)=S_m$ in Eq. (8) which leads to

$$\gamma_L = \frac{(9-64\tau)^{3/4}}{2\sqrt{2}[3-\sqrt{9-64\tau}-8\sqrt{6}S_0/3]}. \quad (12)$$

In the region $(0 < L < \infty)$, the profile has one inflection point [see, e.g., curve (2) in Fig. 4]. When at $\tau=\tau_b$ the vertical part of the wetting line in Fig. 6 is approached, L starts to diverge [see, e.g., curve (3) in Fig. 4]. This is obvious with the help of the graphical solution of Eq. (8): For $S_0 \to 0$ and $\gamma > \sqrt{\tau_b}$ [where $\sqrt{\tau_b}$ is the slope of $\sqrt{f_b(S(0))}$ at $S(0)=0$], $S(0)$ also tends to zero: $S(0) \to 0$. Therefore, a singularity in Eq. (11) for L occurs since $f_b(0)=f_b(S_b)=0$ at $\tau=\tau_b$. Concentrating on the singularity, one finds a logarithmic divergence for L:

$$L \cong \int_{S(0)}^{S_m} \frac{dS}{\sqrt{\tau_b}S} \cong \frac{-1}{\sqrt{\tau_b}} \ln S(0) \quad \text{for } S(0) \to 0. \quad (13)$$

So on approaching the vertical part of the wetting line in the wetting phase diagram (Fig. 6), a second-order transition occurs. The curved part of the wetting line is determined by the Maxwell construction as illustrated in Fig. 3(b) at $\tau=\tau_b$. In the partial-wetting regime, $S(0)$ is positive and L is always finite. When areas 1 and 2 in Fig. 3(b) are equal, $S(0)$ jumps to a negative value and a macroscopically thick film of isotropic phase wets the interface [see the profile (4) in Fig. 4]. So when crossing the curved part of the wetting line, a first-order transition occurs since L jumps to infinity. The Maxwell construction can also be applied to temperatures below τ_b, where it defines the prewetting surface. At τ_b, the surface ends in the curved part of the wetting line and for $\tau < \tau_b$ in a critical line, whose projection on the S_0, γ plane is shown as a dashed line in Fig. 6. When crossing the prewetting surface with decreasing temperature, the thickness L of the wetting layer jumps and ultimately diverges logarithmically on approaching τ_b. The curved and vertical part of the wetting line meet in a tricritical point at $(S_0=0, \gamma=\sqrt{\tau_b}=0.354)$, indicated by the filled square in Fig. 6. Finally, we note that at $\tau=\tau_b$, $f_b(S)$ is symmetric about $S=S_b/2$ [see Fig. 3(b)], which explains why the wetting lines for nematic and isotropic wetting are mirror images of each other. This, however, does not apply to the prewetting surfaces and, especially, their terminating critical lines.

E. Remarks about fitting the experiments

By solving Eq. (10), we obtain an order parameter profile $S(z)$ for each temperature. We then transform $S(z)$ into profiles for the ordinary $[n_o(z)]$ and the extraordinary $[n_e(z)]$ refractive index as described in [18,47], i.e.,

$$n_o^2(z) = n_a^2 + d_\zeta(z)\{[n_{iso}^2 - \tfrac{1}{3}\Delta\epsilon_{max}rS(z)] - n_a^2\}, \quad (14)$$

$$n_e^2(z) = n_a^2 + d_\zeta(z)\{[n_{iso}^2 + \tfrac{2}{3}\Delta\epsilon_{max}rS(z)] - n_a^2\}, \quad (15)$$

with

$$d_\zeta(z) = \frac{1}{2}\left[1 + \tanh\left(\frac{z}{\zeta}\right)\right]. \quad (16)$$

Here, r is the scaling factor from the reduced to the unscaled order parameter, n_a is the refractive index of water, n_{iso} that of the isotropic liquid crystal, and $\Delta\varepsilon_{max} = (n_e^2 - n_o^2)_{max}$ describes the birefringence of the ideally ordered ($rS = 1$) nematic phase. The interface between the aqueous and the organic phase is modeled by a tanh profile of width ζ which is introduced by the function $d_\zeta(z)$.

The ellipsometric parameters $\bar\rho$ and θ_B are calculated following Refs. [48,49]. To perform the necessary integrations, the refractive-index profiles are divided into several hundred layers parallel to the interface with constant indices.

The best fits of the experimental results are obtained from the following Landau parameters: $a_0 = 1.6 \times 10^5$ J m^{-3} K^{-1}, $b = 9.67 \times 10^6$ J m^{-3}, $c = 5.59 \times 10^6$ J m^{-3}, and $L_1 = 4 \times 10^{-11}$ J m^{-1}, which are in good agreement with Coles' work [50]. The values of the optical parameters, $n_{iso} = 1.563$ [51] and $\Delta\varepsilon_{max} = 0.53$ [50], are chosen in accordance with values reported in literature; the interface width ζ is set to 1 nm.

Although the overall agreement between measured and calculated data is quite good, it is not perfect, especially for $T > (T_b + 1$ K$)$ in the samples with larger surfactant concentration [cf. Figs. 2(a) and 2(b)]. A possible reason may be that the phenomenological model is too simple, e.g., the Landau parameters may be weakly temperature dependent. Introducing such a temperature dependence could enhance the agreement between theory and experiment at larger temperature distances to T_b. Another reason could consist of the negligence of the surfactant in our refractive index profiles. The presence of the surfactant molecules at the interfaces results in an additional contribution to $\bar\rho$ which might not be negligible at larger concentrations.

Finally, we should mention that the ellipsometric data shown in Fig. 2(d) are not an unambiguous evidence for a less-ordered nematic layer at the interface. In principle, it would be possible to reproduce the experimental data of Fig. 2(d) using an order parameter profile with a more-ordered nematic surface layer which grows in thickness as T_b is approached from below. Such a behavior, however, would be contradictory to both the theoretical model and the experimental behavior at larger surfactant concentrations, substantiated by Figs. 2(a)–2(c). Furthermore, if surface-enhanced order would exist below T_b, there is no reason why it should be absent just above T_b, as is clearly shown by the data in Fig. 2(d).

IV. DISCUSSION AND CONCLUSIONS

We have studied the behavior of the thermotropic liquid crystal 8CB at surfactant-laden interfaces to aqueous solutions of the surfactant CTAB. The temperature dependence of the ellipticity coefficient $\bar\rho$ and the Brewster angle θ_B was determined for different surfactant concentrations. At higher surfactant concentrations, the interface is completely wetted by a nematic surface phase when T_b is approached from above. With decreasing surfactant concentration, the nematic wetting first becomes partial and finally vanishes. Concurrently, a new wetting behavior, characterized by a considerably decreased nematic order parameter at the interface, develops below T_b. The thickness of this decreased order parameter region grows as T_b is approached from below. The change of the wetting behavior takes place while the type of anchoring remains homeotropic in all samples under investigation.

The scalar order-parameter theory based on the Landau–Ginzburg–de Gennes model supplemented by a surface free energy can reproduce all our experimental observations. To describe the influence of the surfactant concentration, it is sufficient just to change the values of the two surface parameters, anchoring strength γ, and preferred surface order parameter S_0, while all other parameters are held constant.

Although the type of anchoring does not change in our experiment, it is very likely that the observed change from surface-enhanced to surface-decreased order is driven by the approach to an anchoring transition from homeotropic to planar. Since the anchoring on a pure water surface is planar, an anchoring transition must occur at a certain CTAB concentration between 0 and 0.4 μM. Experimental studies [25,26] of the wetting and anchoring behavior of nCB compounds on self-assembled monolayers have suggested that the transition to complete nematic wetting at T_b coincides with an anchoring transition from planar to homeotropic anchoring. In the system of the present study, this is clearly not the case. In this context, it is instructive to consider the path in the γ, S_0 plane, on which the experimental system moves as the surfactant concentration is gradually decreased (cf. Figs. 5 and 6): Reducing the surfactant concentration c_a from 30 μM to 3 μM leads to a considerably decreased anchoring strength γ while the preferred surface order parameter S_0 remains constant. On further decreasing c_a, both parameters, γ and S_0, become smaller and the system crosses a narrow region in which a prewetting transition exists. The 0.7 μM sample still shows continuous complete wetting whereas the 0.6 μM sample is located in the partial wetting region. Careful tuning of the surfactant concentration should enable the experimental realization of a prewetting transition; with the present experimental resolution, however, it might be difficult to observe since the temperature difference to the bulk transition would be of the order of only 50 mK. Decreasing c_a further to 0.4 μM reduces S_0 to almost zero, whereas γ surprisingly increases by a factor of 3 compared to the 0.6 μM sample.

The reason for the unexpected increase of the anchoring strength in the 0.4 μM sample is not obvious. Using data obtained for the adsorption of CTAB at a water–hexadecane interface [52], we can estimate the surfactant coverage Γ of
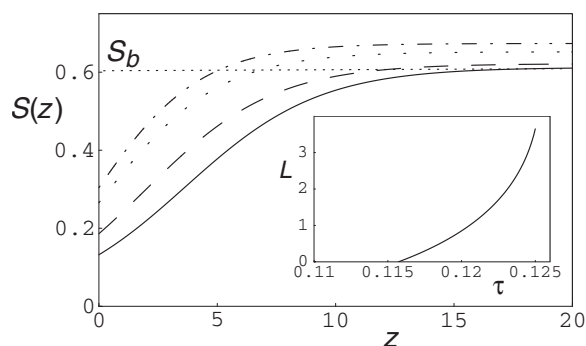
FIG. 7. Order parameter profiles $S(z)$ for the surface-energy parameters $S_0=0.01$ and $\gamma=0.3$ for different temperatures. From the top to the bottom curve, the temperatures are $\tau=0.11$, 0.1158, 0.123, and $\tau_b=0.125$. The inset shows the thickness L of the wetting layer as a function of temperature. The lengths z and L are given in units of $\xi=2.84$ nm.

the interface to amount to ≈ 0.01, i.e., the system is very far from a dense coverage ($\Gamma=1$); nevertheless, the coverage is still sufficient to induce a homeotropic anchoring. On the other hand, the low surfactant coverage could emphasize interactions resulting from the bare water surface which prefers the liquid-crystal molecules to be aligned parallel to the interface. Thus a special situation of competing surfactant and water interactions exists and the observed increase of γ might result from the increasing influence of the bare water surface interactions.

The growth of a disordered surface layer as T_b is approached from below has already been observed for the case of the liquid crystal 5CB on a rough SiO_x substrate which induces a planar unidirectional anchoring of the nematic bulk phase [32]. To our knowledge, we have reported here the first experimental observation of the growth of a disordered surface layer in a liquid crystal system with homeotropic anchoring. Figure 7 shows the order parameter profiles $S(z)$ obtained from fitting the experimental results of the 0.4 μM sample; the $S(z)$ profiles illustrate the growth of the interface layer with decreased nematic order parameter as T_b is approached from below. In the γ, S_0 plane, the 0.4 μM sample is still located in the partial wetting region (although very close to the transition line to complete wetting), i.e., the less-ordered surface layer retains a finite width at T_b. The Landau model predicts complete wetting by a less-ordered surface phase only for $S_0 \leqslant 0$. In that case, an isotropic surface phase would develop if the temperature is sufficiently close to T_b (cf. Fig. 4). A corresponding experimental system, however, would be difficult to study with the present experimental setup which requires a homeotropic anchoring; this condition is no longer assured when an isotropic phase intrudes between the nematic bulk phase and the aqueous phase.

ACKNOWLEDGMENTS

[1] B. Jérôme, Rep. Prog. Phys. **54**, 391 (1991).
[2] G. P. Crawford, R. J. Ondris-Crawford, J. W. Doane, and S. Žumer, Phys. Rev. E **53**, 3647 (1996).
[3] P. Sheng, Phys. Rev. A **26**, 1610 (1982).
[4] T. J. Sluckin and A. Poniewierski, Phys. Rev. Lett. **55**, 2907 (1985).
[5] A. K. Sen and D. E. Sullivan, Phys. Rev. A **35**, 1391 (1987).
[6] H. Stark, J. Fukuda, and H. Yokoyama, J. Phys.: Condens. Matter **16**, S1911 (2004).
[7] J.-B. Fournier and P. Galatola, Europhys. Lett. **72**, 403 (2005).
[8] M. M. Telo da Gama, Mol. Phys. **52**, 611 (1984).
[9] J. H. Thurtell, M. M. Telo da Gama, and K. E. Gubbins, Mol. Phys. **54**, 321 (1985).
[10] Z. Pawlowska, T. J. Sluckin, and G. F. Kventsel, Phys. Rev. A **38**, 5342 (1988).
[11] B. Tjipto-Margo, A. K. Sen, L. Mederos, and D. E. Sullivan, Mol. Phys. **67**, 601 (1989).
[12] A. M. Somoza, L. Mederos, and D. E. Sullivan, Phys. Rev. E **52**, 5017 (1995).
[13] E. M. del Rio, M. M. Telo da Gama, E. de Miguel, and L. F. Rull, Phys. Rev. E **52**, 5028 (1995).
[14] I. Rodriquez-Ponce, J. M. Romero-Enrique, E. Velasco, L. Mederos, and L. F. Rull, Phys. Rev. Lett. **82**, 2697 (1999).
[15] D. Beaglehole, Mol. Cryst. Liq. Cryst. **89**, 319 (1982).
[16] B. M. Ocko, A. Braslau, P. S. Pershan, J. Als-Nielsen, and M. Deutsch, Phys. Rev. Lett. **57**, 94 (1986).
[17] P. de Schrijver, C. Glorieux, W. van Dael, and J. Thoen, Liq. Cryst. **23**, 709 (1997).
[18] R. Lucht, Ch. Bahr, and G. Heppke, Phys. Rev. E **62**, 2324 (2000).
[19] K. Miyano, Phys. Rev. Lett. **43**, 51 (1979).
[20] H. Yokoyama, S. Kobayashi, and H. Kamei, Appl. Phys. Lett. **41**, 438 (1982).
[21] H. Yokoyama, S. Kobayashi, and H. Kamei, Mol. Cryst. Liq. Cryst. **99**, 39 (1983).
[22] H. Hsiung, Th. Rasing, and Y. R. Shen, Phys. Rev. Lett. **57**, 3065 (1986).
[23] W. Chen, L. J. Martinez-Miranda, H. Hsiung, and Y. R. Shen, Phys. Rev. Lett. **62**, 1860 (1989).
[24] B. M. Ocko, Phys. Rev. Lett. **64**, 2160 (1990).
[25] B. Alkhairalla, H. Allinson, N. Boden, S. D. Evans, and J. R. Henderson, Phys. Rev. E **59**, 3033 (1999).
[26] B. Alkhairalla, N. Boden, E. Cheadle, S. D. Evans, J. R. Henderson, H. Fukushima, S. Miyashita, H. Schönherr, G. J. Vancso, R. Colorado, M. Graupe, O. E. Shmakova, and T. R. Lee, Europhys. Lett. **59**, 410 (2002).
[27] K. Kočevar and I. Muševič, Phys. Rev. E **65**, 021703 (2002).
[28] M. I. Boamfa, M. W. Kim, J. C. Maan, and Th. Rasing, Nature (London) **421**, 149 (2003).
[29] G. S. Iannacchione, J. T. Mang, S. Kumar, and D. Finotello,

Phys. Rev. Lett. **73**, 2708 (1994).

[30] P. Ziherl, M. Vilfan, N. Vrbančič-Kopač, S. Žumer, R. J. Ondris-Crawford, and G. P. Crawford, Phys. Rev. E **61**, 2792 (2000).

[31] T. Jin, G. P. Crawford, R. J. Crawford, S. Zumer, and D. Finotello, Phys. Rev. Lett. **90**, 015504 (2003).

[32] T. Moses and Y. R. Shen, Phys. Rev. Lett. **67**, 2033 (1991).

[33] J. M. Brake, A. D. Mezera, and N. L. Abbott, Langmuir **19**, 6436 (2003).

[34] Ch. Bahr, Phys. Rev. E **73**, 030702(R) (2006).

[35] P. G. de Gennes and J. Prost, *The Physics of Liquid Crystals*, 2nd ed. (Oxford Science Publications, Oxford, 1993).

[36] A. Saupe, Z. Naturforsch. A **19a**, 161 (1964).

[37] P. G. de Gennes, Phys. Lett. **30A**, 454 (1969).

[38] T. C. Lubensky, Phys. Rev. A **2**, 2497 (1970).

[39] S. Hess, Z. Naturforsch. A **30a**, 728 (1975).

[40] P. G. de Gennes, Mol. Cryst. Liq. Cryst. **12**, 193 (1971).

[41] Landau–Ginzburg–de Gennes free energy density in the one-constant approximation for the elastic energy: $f(\mathbf{Q}) = \frac{1}{2}a_0(T - T^*)Q_{ij}Q_{ij} - \frac{1}{3}bQ_{ij}Q_{jk}Q_{ki} + \frac{1}{4}c(Q_{ij}Q_{ij})^2 + \frac{1}{2}L_1(Q_{ij,k})^2$, where summation over repeated indices is implied and the symbol k means spatial derivative with respect to the spatial coordinate x_k.

[42] N. Kothekar, D. W. Allender, and R. M. Hornreich, Phys. Rev. E **49**, 2150 (1994).

[43] R. M. Hornreich, E. I. Kats, and V. V. Lebedev, Phys. Rev. A **46**, 4935 (1992).

[44] Y. L'vov, R. M. Hornreich, and D. W. Allender, Phys. Rev. E **48**, 1115 (1993).

[45] R. Seidin, R. M. Hornreich, and D. W. Allender, Phys. Rev. E **55**, 4302 (1997).

[46] M. Huber and H. Stark, Europhys. Lett. **69**, 135 (2005).

[47] S. Immerschitt, T. Koch, W. Stille, and G. Strobl, J. Chem. Phys. **96**, 6249 (1992).

[48] A. W. Crook, J. Opt. Soc. Am. **38**, 954 (1948).

[49] R. M. A. Azzam and N. M. Bashara, *Ellipsometry and Polarized Light* (North-Holland, Amsterdam, 1989).

[50] H. J. Coles, Mol. Cryst. Liq. Cryst. **49**, 67 (1978).

[51] P. P. Karat and N. V. Madhusudana, Mol. Cryst. Liq. Cryst. **36**, 51 (1976).

[52] M. M. Knock, G. R. Bell, E. K. Hill, H. J. Turner, and C. D. Bain, J. Phys. Chem. B **107**, 10801 (2003).